Cosmological Filaments and Minivoids: The Origin of Intergalactic Absorption[#]

Yu Zhang[†*], Avery Meiksin[‡], Peter Anninos[†], & Michael L. Norman[†*]

[†]*Laboratory for Computational Astrophysics*
National Center for Supercomputing Applications
University of Illinois at Urbana-Champaign
405 N. Mathews Ave., Urbana, IL 61801

[‡]*Edwin Hubble Research Scientist*
University of Chicago
Department of Astronomy & Astrophysics
5640 South Ellis Avenue
Chicago, IL 60637

Soon after the first QSO was identified, Gunn & Peterson[1] searched for the expected characteristic absorption trough on the blueward side of Lyα in the spectrum of the QSO due to an Intergalactic Medium (IGM). They failed to find it, placing a constraint on the density of neutral hydrogen in the IGM that was less than 1 part in 10^5 of that residing in galaxies, and concluded that the IGM must be highly ionized. Soon afterwards absorption by Lyα was detected in the IGM; not by a diffuse component, but by a clumpy component of intergalactic gas clouds, the Lyα forest[2,3]. The goal then became to search for 'excess' absorption beyond that expected from the forest. No clear absorption by a diffuse H I component, however, was ever detected[4,5]. The results of recent numerical hydrodynamics computations of the formation of the Lyα forest appear to indicate that the division between a clumpy component and a diffuse one may be inappropriate. We find that in a CDM-dominated cosmology, no substantial diffuse medium should be expected. Instead, the medium condenses into a network of complex structures that reveal themselves as discrete absorption systems in the spectra of QSOs. The lowest column density lines arise from the fine structure in minivoids – small regions with densities below the cosmic mean. These results suggest that the long sought for diffuse H I Gunn-Peterson effect may not exist.

Submitted to *Nature*

* *Astronomy Department, University of Illinois at Urbana-Champaign*

Recent ground and space measurements of intergalactic absorption in the spectra of high redshift QSOs have considerably expanded our knowledge of the structure of the IGM. Keck observations[6,7] have revealed that the forest extends to H I column densities as low as $N_{\rm HI} \sim 10^{12}\,{\rm cm}^{-2}$, while the *Hubble Space Telescope*[8] and the *Hopkins Ultraviolet Telescope* (Davidsen et al., submitted to *Nature*), have made the first detections of intergalactic He II . The Keck data show no conspicuous absorption by a diffuse H I component at $z \sim 3$. Absorption by diffuse He II in the IGM is expected to be more easily detected than H I because of its higher density, however it is unclear whether the He II detections were of a diffuse component or of the He II content of the Lyα forest[9]. Indeed, Keck observations suggest the latter may account for the measured opacity without invoking an unreasonably steep photoionizing background radiation field.[9,10] In agreement with ground based H I observations, no diffuse component appears to be required.

We analyze the results of a recent cosmological hydrodynamics simulation of the formation of the Lyα forest in a Cold Dark Matter (CDM) dominated cosmology by Zhang, Anninos & Norman[11] and derive their implications for H I and He II absorption. For much of our discussion, we have rescaled the ionization fractions to the metagalactic radiation field recently determined by Haardt and Madau[12] (HM) on the basis of QSO counts, including the re-emission from the forest and Lyman-limit systems. The rescaling should have little impact on the cloud properties other than on their ionization state, at least for the column density range of interest here. We show the distribution of gas density in Figure 1. For the density threshold shown, the IGM appears as a network of filaments, with a typical coherence length of 1–2 Mpc and thickness 100–200 kpc. These scales are comparable to the recent size estimates based on neighboring QSO pairs[13,14]. In between the filaments are underdense regions, or cosmic 'minivoids.'

To translate the H I density into spectra, we lay down random lines of sight through the box and determine the absorption features that would be observed in a background QSO. We then identify absorption features with optical depths exceeding 0.2, de-blend the features into individual lines, fit the lines and extract the column densities and Doppler widths using a curve-of-growth analysis, as described by Zhang, Anninos, Norman, & Meiksin (in preparation). The column density distribution matches the observed distribution in shape remarkably well, as has been found in other simulations for CDM (Hernquist *et al.* submitted to *Astrophys. J*) and CDM + Λ[15] cosmologies. The number of systems per unit column density varies as a power law, $dN/dN_{\rm HI} \propto N_{\rm HI}^{-\beta}$, with $\beta \simeq 1.5$ for $N_{\rm HI} < 10^{14}\,{\rm cm}^{-2}$, in agreement with findings from the Keck[7]. There is an essential uncertainty in the H I column densities, however, resulting from the unknown ionization fractions. The neutral fraction is proportional to $b_{\rm ion} \equiv (\Omega_b h_{50}^2)^2/J_{912}$ (for clouds optically thin at the H I Lyman edge), where J_{912} is the background intensity at the H I Lyman edge. This acts effectively as an 'ionization bias' relating the neutral hydrogen column density of an absorber to its total hydrogen column density. Defining $b_{\rm ion} = 1$ for $\Omega_b h_{50}^2 = 0.06$ and the HM value for the background intensity, we find that rescaling the background radiation to $b_{\rm ion} = 1.5$ matches the number density of $N_{\rm HI} > 10^{13}\,{\rm cm}^{-2}$ systems measured by the Keck[7] at $z = 3$. We assume this value throughout. It is noteworthy that this value would place the required Ω_b close to the nucleosynthesis upper limit[16] of $\Omega_b h_{50}^2 < 0.08$ for the HM spectrum. If the metagalactic radiation field much exceeds the estimated contribution from QSOs, or if the density of baryons is lower, as suggested by some recent deuterium measurements in high redshift absorption systems[17], then this cosmological model would appear to be in conflict with the measured numbers of clouds in the Lyα forest.

A wide range of local densities is responsible for the absorbers. In Figure 2 we show the average column density as a function of the local average density, normalized by the average cosmological value. Those systems which are optically thin at line-center arise in minivoids. In fact, we find that at redshift $z = 3$ more than 70% of the baryons reside in overdense regions, while the remainder, in underdense regions, produces most of the low column density ($10^{11} - 10^{13}$ cm^{-2}) systems. These results suggest that the long sought for diffuse component of the IGM may not exist, but that clumping is ubiquitous, even in regions at the average cosmic density and below. The view that QSOs dominate the background UV radiation field and that the Lyα forest captures most of the baryons at $z > 2$ is fully consistent with current observations[18,12]. This view differs dramatically from the prevailing model of the IGM in which the Lyα forest is composed of clouds embedded in a pervasive diffuse medium that survived the onset of structure formation at high redshift and contained the majority of the baryons created during the Big Bang.

Most of the absorption in a QSO spectrum shortward of Lyα results from line-blanketing, the stochastic overlapping of absorption features. Searches for the Gunn-Peterson effect have been attempts to detect excess absorption above that due to the forest[4,5]. Since the forest extends to very low column densities, however, the distinction between the two becomes somewhat semantic. But while line-blanketing and optically thin 'Gunn-Peterson' absorption are related, they are not identical. The connection may be made concrete by appealing to the effective opacity $\tau_{\rm eff}$, defined by $\exp(-\tau_{\rm eff}) = \langle\exp(-\tau_\nu)\rangle$. For line-blanketing[19],

$$\tau_{\rm eff} \equiv \frac{1+z}{\lambda_0}\int dW \frac{\partial^2 N}{\partial z \partial W} W, \tag{1}$$

for a cloud distribution of redshifts and rest-frame equivalent widths $\partial^2 N/\partial z\partial W$. Restricting the range to optically thin clouds at line-center gives $\tau_{\rm eff} \rightarrow \tau_{\rm GP}^{\rm thin}$, where $\tau_{\rm GP}^{\rm thin}$ is the Gunn-Peterson opacity corresponding to the spatially averaged neutral hydrogen density $\langle n_{\rm HI}^{\rm thin}\rangle$ of the optically thin systems[20,1],

$$\tau_{\rm GP}^{\rm thin} = \frac{s_u \lambda_0}{H_0} \frac{\langle n_{\rm HI}^{\rm thin}\rangle}{(1+z)(1+2q_0 z)^{1/2}}, \tag{2}$$

where s_u is the frequency integrated absorption cross-section[21]. According to Figure 2, clouds of unit optical depth correspond to regions near the average cosmological baryon density. Thus, we may identify the H I Gunn-Peterson effect with the optically thin tail of the Lyα forest. By contrast, the opacity resulting from the high column density systems measures the product of the Doppler parameter of the clouds and their number per unit line-of-sight, above a given column density, or line-center opacity, threshold. This is because an optically thick cloud enters the flat part of the curve-of-growth, for which the equivalent width is proportional to the Doppler width and insensitive to the H I density. (Note, though, that the number of clouds above a fixed opacity threshold is sensitive to the internal cloud H I density.) The physical distinction in the character of these two limits may be exploited to test two different aspects of the nature of the clouds and their evolution. In Figure 3a, we show the evolution of $\tau_{\rm eff}$ for optically thin ($0.2 < \tau_0 < 1$ and $0.5 < \tau_0 < 1$) and optically thick ($\tau_0 > 10$) systems. We also show the contribution from all the clouds with $\tau_0 > 0.2$. (Only clouds optically thin at the Lyman edge are counted since we have not corrected for radiative transfer effects.) We find good agreement with the expected amount of blanketing inferred from observations over the limited redshift range currently available.

A quantity closely related to the effective opacity is D_A, the flux decrement in a QSO spectrum between Lyα and Lyβ [22],

$$D_A = \frac{5}{32}\frac{1}{(1+z_Q)}\int_{(27/32)(1+z_Q)-1}^{z_Q}\left[1-\exp(-\tau_\nu)\right]dz, \tag{3}$$

where z_Q is the redshift of the QSO. In Figure 3b, we show the evolution of D_A obtained from the simulation, including cuts based on overdensity. The distinction between the optically thin and optically thick absorbers is clear: the absorption due to the optically thin material, occupying regions near the average cosmic density, behaves like the Gunn-Peterson opacity for $\tau_{GP} \ll 1$. We also compute D_B, the decrement between Lyβ and the Lyman limit[22]. We find $D_B/D_A = (1.1, 1.2, 1.2, 3.3)$ for $z = (2, 3, 4, 5)$, compared to the average measured ratios[23,24] of 1.5 at $z = 3$ and 1.2 at $z = 4$.

The recent determinations of the He II Lyα opacity, τ_{304}, may be used to constrain the shape of the background UV radiation field[8–10]. The He II opacity predicted, however, requires an extrapolation of the H I column density distribution to lower than measured values as well as knowledge of the unmeasured He II Doppler parameters[9]. These quantities are predicted by the simulation, and so it is of interest to infer the constraint on the radiation field the simulation implies. In Figure 4, we show the evolution of τ_{304} for different values of the softness parameter $S_L \equiv J_{912}/J_{228}$, the ratio of intensities at the H I and He II Lyman edges. We find that in order to match the observed values, $S_L > 60$ is required, a value consistent with a QSO-dominated UV background, though for a somewhat soft intrinsic QSO spectrum ($\alpha \gtrsim 1.5$)[9]. A He II opacity of $\tau_{304} > 2$ at $z = 3$ would be difficult to reconcile with a QSO dominated background. It would then be necessary to appeal to additional sources of H I ionization, like an early generation of stars or decaying neutrinos[26].

We point out that substantial fluctuations in the opacity are expected on small scales, as shown in Figure 1. These fluctuations result from the large density fluctuations expected on small scales in a CDM cosmology. While most of the H I blanketing arises from systems in regions near the average cosmological density, the He II blanketing is dominated by the smaller scale systems in the underdense regions. The He II opacity thus serves as a probe of the minivoids.

We conclude that the IGM may be highly clumped, with a negligible baryon fraction residing in a diffuse component. It is for this reason that a diffuse component may have evaded detection in the form of the Gunn-Peterson effect. The canonical picture of the IGM in which the absorption clouds are embedded in a diffuse background medium is not viable in a CDM dominated cosmology. It is replaced by a continuous spectrum of clumpiness: from the high overdensity halos which give rise to the high column density absorption lines, to the mildly overdense filaments which give rise to the intermediate column density absorbers, to the underdense minivoids which are responsible for most of the low column density systems that have just recently been discovered.

Figure Captions

Fig. 1. — Distribution of the gas density at $z = 3$ from a numerical hydrodynamics simulation of the Lyα forest. The simulation adopted a CDM spectrum of primordial density fluctuations, normalized to the second year COBE observations, a Hubble constant of $H_0 = 50\,\mathrm{km\,s^{-1}\,Mpc^{-1}}$, a comoving box size of 9.6 Mpc, and baryonic density of $\Omega_b = 0.06$ composed of 76% hydrogen and 24% helium. The region shown is 2.4 Mpc (proper) on a side. The isosurfaces represent baryons at ten times the mean cosmic density (characteristic of typical filamentary structures) and are color coded to the gas temperature (dark blue = 3×10^4 K, light blue = 3×10^5 K). We note that higher density contours trace out isolated spherical structures typically found at the intersections of the filaments. A single random slice through the cube is also shown, with the baryonic overdensity represented by a rainbow–like color map changing from black (minimum) to red (maximum). The He II mass fraction is shown with a wire mesh in this same slice. Notice that there is fine structure everywhere. To emphasize the fine structure in the minivoids, we have rescaled the mass fraction in the overdense regions by the gas overdensity wherever it exceeds unity.

Fig. 2. — Distribution of H I column density of the clouds as a function of the local baryon overdensity. The vertical solid line is the dividing line between the overdense and underdense regions. The horizontal dashed line represents the column density $N_{\mathrm{HI}} = 10^{16.9}$ cm^{-2} above which the H I opacity at the Lyman edge exceeds 0.5 and radiation transport effects become important. Discrete absorption systems exhibit the full range of densities, and arise even in regions that are underdense. The clouds become optically thin in Lyα at line-center for $N_{\mathrm{HI}} \lesssim 10^{13}$ cm^{-2}. Optically thin systems occur predominantly in the underdense regions, although there is a smooth transition between optically thin and thick absorbers.

Fig. 3. — (a) Effective opacity τ_{eff} for optically thin ($0.2 < \tau_0 < 1$ and $0.5 < \tau_0 < 1$) and optically thick ($\tau_0 > 10$) Lyα clouds. (A lower limit of $\tau_0 > 0.5$ for the thin systems is required to avoid incompleteness in the Keck data.) While the optically thin opacity traces the spatially averaged neutral H I density of the clouds, the opacity based on the optically thick systems traces the Doppler width and number of the clouds per unit line-of-sight, since the equivalent width of a saturated line is given by[21] $W \simeq (2b/c)\lambda_0(\log \tau_0)^{1/2}$, nearly independent of τ_0, the line center opacity. These opacities test independent properties of the clouds, and both agree closely with the measured values from Keck observations[7]. We also show the full contribution of all the lines with $\tau_0 > 0.2$ to the effective opacity. These values again agree well with the estimate from the Keck data. (b) H I flux decrement $\mathrm{D_A}$ due to H I Lyα absorption. The contributions from several overdensity cuts are shown separately, corresponding closely to cuts in H I column density. The measured values[23–25] compare well with the simulation results. We note that the agreement for $z > 3$ may be improved by allowing for an additional contribution to the UV background from QSOs obscured by dust in damped Lyα systems[27]. The thin solid line shows the contribution to $\mathrm{D_A}$ from the lines, computed as $\mathrm{D_L} = 1 - \exp(-\tau_{\mathrm{eff}})$. This indicates that the decrement is due almost entirely to line-blanketing. Also shown (dotted line) is the Gunn-Peterson opacity obtained by summing the contribution to the absorption from underdense regions as in equation (2), and expressed as a flux decrement $\mathrm{D_{GP}}$. The Gunn-Peterson value correlates strongly with the contribution of the underdense material to $\mathrm{D_A}$ for $\tau_{\mathrm{GP}} \ll 1$, demonstrating that the H I in the underdense regions is optically thin in Lyα . Accordingly, the absorption arising

from the underdense regions may be associated with the Gunn-Peterson effect. Its small value reflects the small fraction of the baryons residing in the underdense regions.

Fig. 4. — He II Lyα opacity using the numerical data rescaled by the Haardt & Madau[12] radiation spectrum, with $b_{\rm ion} = 1.5$. We reduce the He II spectrum amplitude with respect to the H I by factors of 2, 5 and 10 over the HM spectrum, corresponding to softness parameters of $S_L = 60$, 200 and 400 respectively. The cross is the 1σ result of 3.2, with an error of $(+\infty, -1.1)$, at $z = 3.2$ from the *HST FOC* observation of Jakobsen et al.[8] and the filled square is their 90% confidence lower limit of 1.7. The filled circle is from the *ASTRO-2 HUT* observation of Davidsen et al. (submitted to *Nature*) of 1.00 ± 0.07 at an average redshift $< z >= 2.4$.

1. Gunn, J. E. & Peterson, B. A. Astrophys. J. 142, 1633–1636 (1965).

2. Lynds, C. R. Astrophys. J. 164, L73–L78 (1971).

3. Sargent, W. L. W., Young, P. J., Boksenberg, A. & Tytler, D. Astrophys. J. Suppl. Ser. 42, 41–81 (1980).

4. Steidel, C. C. & Sargent, W. L. W. Astrophys. J. 318, L11-L13 (1987).

5. Giallongo, E., D'Odorico, S., Fontana, A., McMahon, R. G., Savaglio, S., Cristiani, S., Molaro, P. & Trevese, D. Astrophys. J. 425, L1–L4 (1994).

6. Tytler, D., Fan, X.-M., Burles, S., Cottrell, L., Davis, C., Kirkman, D. & Zuo, L. in *QSO Absorption Lines* (ed. Meylan, G.) (Springer, 1995).

7. Hu, E. M., Kim, T.-S., Cowie, L. L., Songaila, A. & Rauch, M. Astron. J. 110, 1526–1543 (1995).

8. Jakobsen, P., Boksenberg, A., Deharveng, J. M., Greenfield, P., Jedrzejewski, R. & Paresce, F. Nature 370, 35–39 (1994).

9. Madau, M. & Meiksin, A. Astrophys. J. 433, L53–L56 (1994).

10. Songaila, A., Hu, E. M. & Cowie, L. L. Nature, L124–L126 (1995).

11. Zhang, Y., Anninos, P. & Norman, M. L. Astrophys. J. 453, L57–L60 (1995).

12. Haardt, F. & Madau, P. Astrophys. J. (in press) (1996).

13. Dinshaw, N., Foltz, C. B., Impey, C. D., Weymann, R. J. & Morris, S. L. Nature 373, 223–225 (1995).

14. Smette, A., Surdej, J., Shaver, P. A., Reimers, D., Wisotzki, L. & Köhler, T. Astr. & Astrophys. (in press) (1996).

15. Cen, R., Miralda-Escude, J., Ostriker, J. P. & Rauch, M. Astrophys. J. 437, L9–L12 (1994).

16. Copi, C. J., Schramm, D. N. & Turner, M. S. Astrophys. J. 455, L95–L98 (1995).

17. Songaila, A., Cowie, L. L., Hogan, C. J., and Rugers, M. Nature, 368, 599-604 (1994).

18. Meiksin, A. & Madau, P. Astrophys. J. 412, 34–55 (1993).

19. Press, W. H., Rybicki, G. B. & Schneider, D. P. Astrophys. J. 414, 64–81 (1993).

20. Field, G. B. Astrophys. J. 129, 536–550 (1959).

21. Spitzer, L. *Physical Processes in the Interstellar Medium* (John Wiley & Sons, 1978).

22. Oke, J. B. & Korycansky, D. G. Astrophys. J. 255, 11–19 (1982).

23. Steidel, C. L. & Sargent, W. L. W. Astrophys. J. 313, 171–184 (1987).

24. Schneider, D. P., Schmidt, M. & Gunn, J. E. Astron. J. 101, 2004–2016 (1991).

25. Kennefick, J. D., deCarvalho, R. R., Djorgovski, S. G., Wilber, M. M., Dickson, E. S., Weir, N., Fayyad, U. & Roden, J. Astron. J. 110, 78–86 (1995).

26. Sciama, D. W. *Modern Cosmology and the Dark Matter Problem* (Cambridge University Press, 1993).

27. Fall, S. M. & Pei, Y. C. Astrophys. J. 402, 479–492 (1993).

ACKNOWLEDGEMENT. We are very grateful to John Shalf for his help in producing Figure 1. This work is supported in part by NSF under the auspices of the Grand Challenge Cosmology Consortium (GC3). A.M. is grateful to the NCSA at UIUC for its hospitality where part of this work was conducted and to the W. Gaertner Fund at the University of Chicago for support. The calculations were performed on the Convex C3880 system

at the National Center for Supercomputing Applications, University of Illinois at Urbana-Champaign.

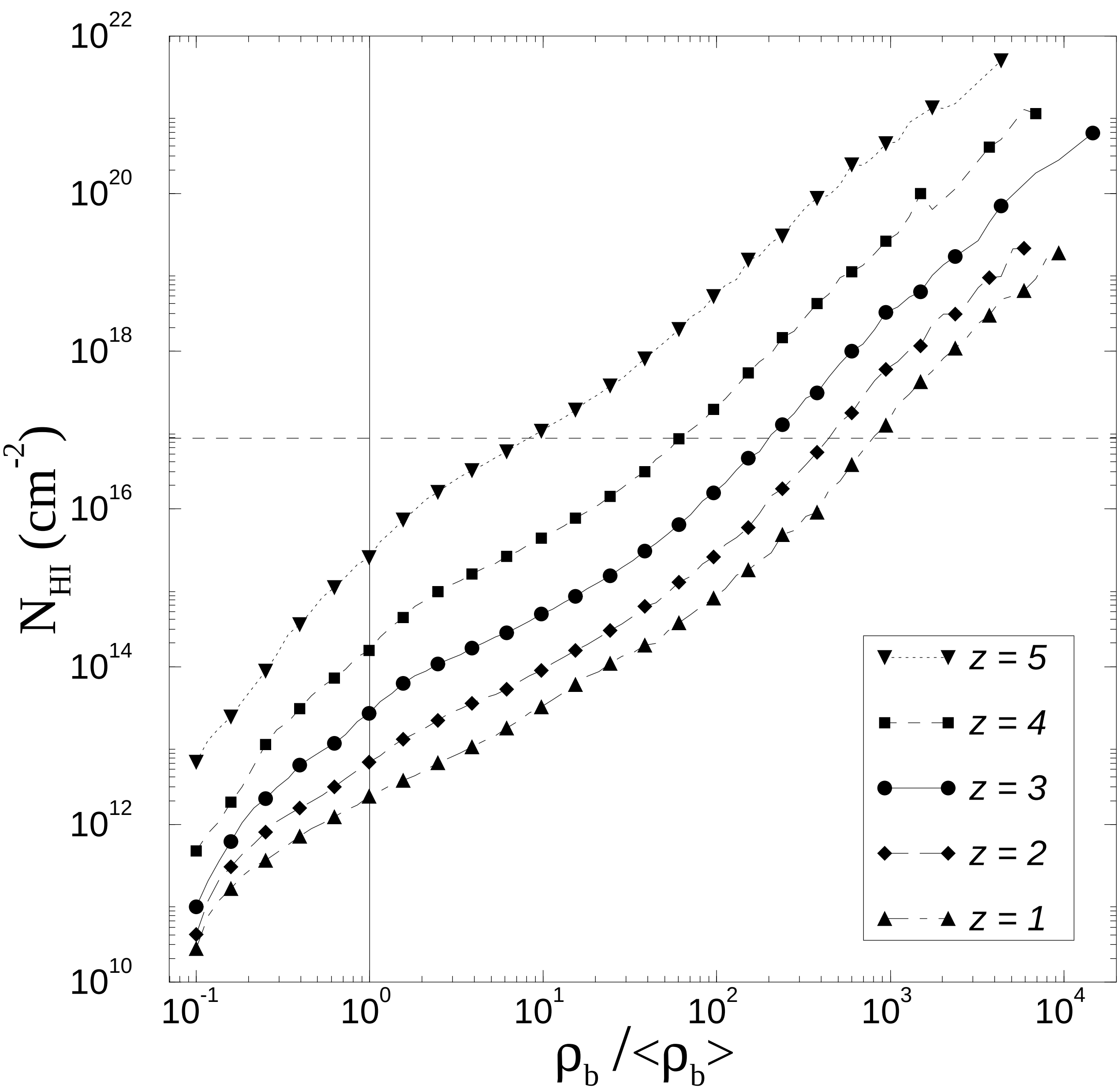

10^{22}
10^{20}
10^{18}
10^{16}
10^{14}
10^{12}
10^{10}
N_{HI} (cm^{-2})
10^{-1}
10^{0}
10^{1}
10^{2}
10^{3}
10^{4}
$\rho_b / \langle\rho_b\rangle$
$z = 5$
$z = 4$
$z = 3$
$z = 2$
$z = 1$

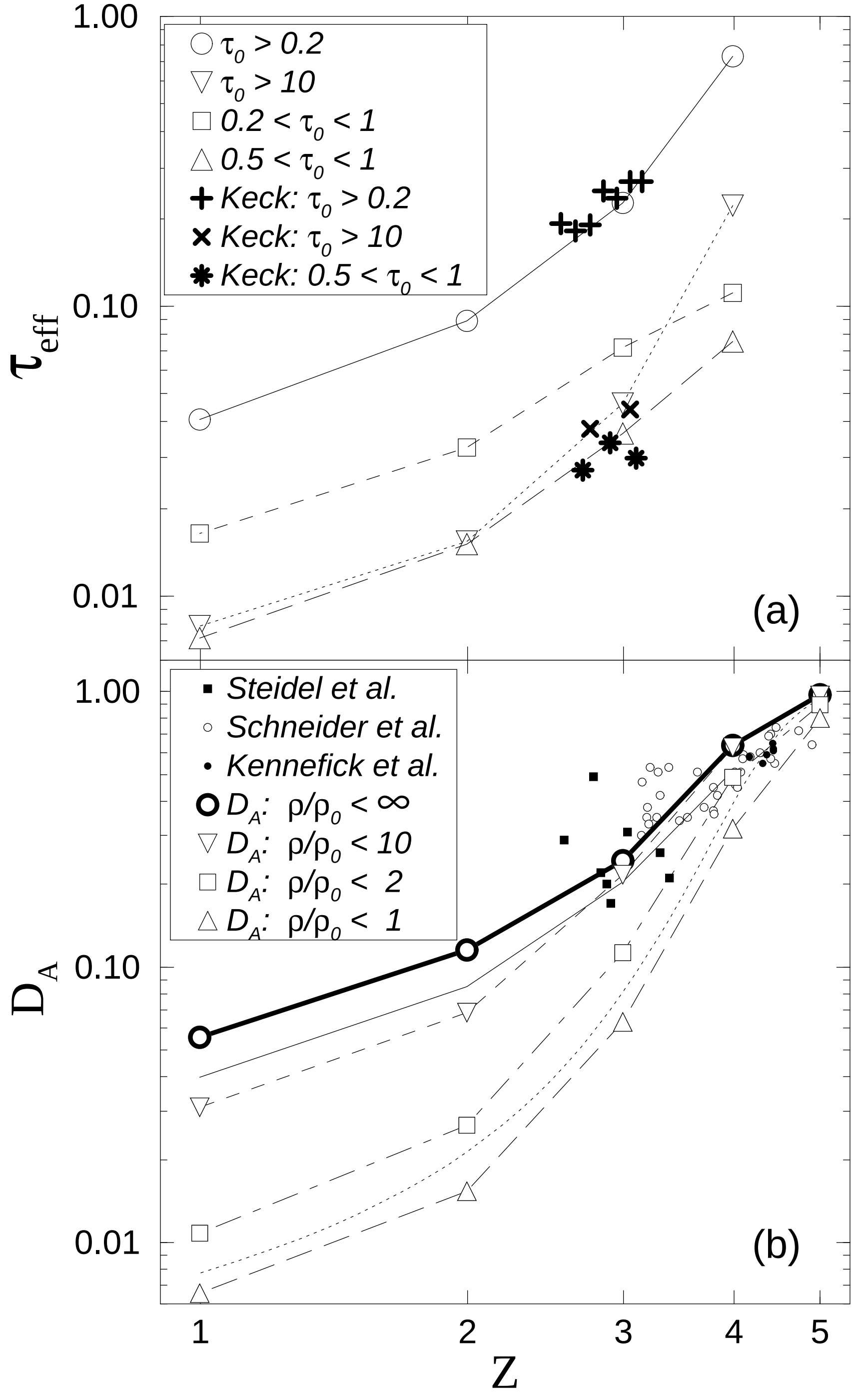

$\tau_0 > 0.2$
$\tau_0 > 10$
$0.2 < \tau_0 < 1$
$0.5 < \tau_0 < 1$
Keck: $\tau_0 > 0.2$
Keck: $\tau_0 > 10$
Keck: $0.5 < \tau_0 < 1$
τ_{eff}
(a)
Steidel et al.
Schneider et al.
Kennefick et al.
D_A: $\rho/\rho_0 < \infty$
D_A: $\rho/\rho_0 < 10$
D_A: $\rho/\rho_0 < 2$
D_A: $\rho/\rho_0 < 1$
D_A
(b)
Z

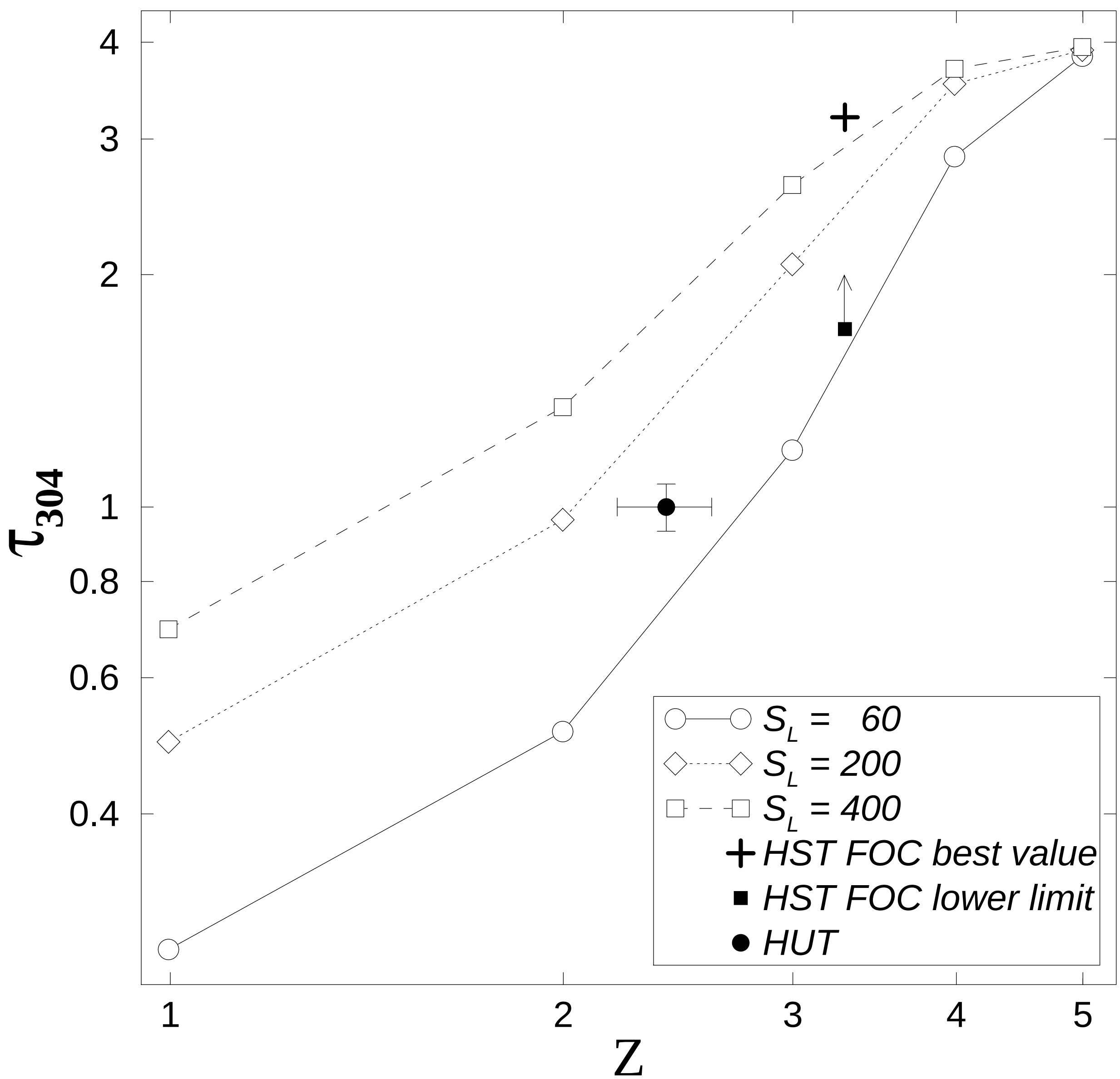

τ_{304}
Z
4
3
2
1
0.8
0.6
0.4
1
2
3
4
5
S_L = 60
S_L = 200
S_L = 400
HST FOC best value
HST FOC lower limit
HUT